Eur Biophys J (2013) 42:463–476
DOI 10.1007/s00249-013-0897-x

ORIGINAL PAPER

EBSA
Biophysics in Europe

Analytical ultracentrifugation studies of oligomerization and DNA-binding of TtCarH, a *Thermus thermophilus* coenzyme B_{12}-based photosensory regulator

Ana I. Díez · Juan Manuel Ortiz-Guerrero · Alvaro Ortega · Montserrat Elías-Arnanz · S. Padmanabhan · José García de la Torre

Received: 21 December 2012 / Revised: 25 February 2013 / Accepted: 27 February 2013 / Published online: 20 March 2013

Abstract *Thermus thermophilus* transcriptional factor TtCarH belongs to a newly discovered class of photoreceptors that use 5′-deoxyadenosylcobalamin ($AdoB_{12}$) as the light-sensing chromophore. Photoregulation relies on the repressor activity of $AdoB_{12}$-bound oligomers in the dark, which light counteracts by oligomer disruption due to $AdoB_{12}$ photolysis. In this study, we investigated TtCarH self-association and binding to DNA in the dark and in the light using analytical ultracentrifugation (AUC) methods, both sedimentation velocity (SV) as well as equilibrium (SE). From a methodological point of view, this study shows that AUC can provide hydrodynamic insights in cases where light is a crucial determinant of solution properties. For the light-sensitive TtCarH, absorbance as well as interference AUC data yielded comparable results. Sedimentation coefficients and whole-body hydrodynamic analysis from SV experiments indicate that in solution apo-TtCarH and light-exposed $AdoB_{12}$–TtCarH are predominantly aspherical, ellipsoidal monomers, in accord with SE data. By comparison, $AdoB_{12}$–TtCarH exists as a more compact tetramer in the dark, with smaller forms such as dimers or monomers remaining undetected and low levels of larger oligomers appearing at higher protein concentrations. AUC analyses indicate that in the dark $AdoB_{12}$–TtCarH associates as a tetramer with DNA but forms smaller complexes in the apo form or if exposed to light. The self-association and DNA-binding properties of TtCarH deduced from AUC are consistent with data from size-exclusion and DNA-binding gel-shift assays. AUC analyses together with hydrodynamic modeling provide insights into the $AdoB_{12}$- and light-dependent self-association and DNA-binding of TtCarH.

Keywords Analytical ultracentrifugation · Hydrodynamics · Light-dependent self-association · CarH · *Thermus thermophilus*

A. I. Díez · A. Ortega · J. García de la Torre (✉)
Departamento de Química Física, Facultad de Química, Universidad de Murcia, 30071 Murcia, Spain
e-mail: jgt@um.es

J. M. Ortiz-Guerrero · M. Elías-Arnanz
Departamento de Genética y Microbiología, Área de Genética (Unidad Asociada al IQFR-CSIC), Facultad de Biología, Universidad de Murcia, 30071 Murcia, Spain

J. M. Ortiz-Guerrero · S. Padmanabhan (✉)
Instituto de Química Física "Rocasolano", Consejo Superior de Investigaciones Científicas, Serrano 119, 28006 Madrid, Spain
e-mail: padhu@iqfr.csic.es

Introduction

Vitamin B_{12} (cobalamin), a large and complex cobalt-containing tetrapyrrole derivative that is essential in humans and other animals but is synthesized exclusively by microorganisms (Croft et al. 2005; Roth et al. 1996; Taga et al. 2007; Warren et al. 2002), is best known as a cofactor of enzymes such as isomerases, methyltransferases, and reductases (Banerjee and Ragsdale 2003; Ludwig and Matthews 1997) and of the B_{12} riboswitch, an RNA-based element implicated in gene regulation (Johnson et al. 2012; Nahvi et al. 2002; Peselis and Serganov 2012). Recently, we described two novel bacterial photosensory regulators, CarH in *Myxococcus xanthus* and TtCarH in *Thermus thermophilus*, that use B_{12} as the light-sensing chromophore (Ortiz-Guerrero et al. 2011). Both are transcriptional regulators that control expression from a light-inducible promoter to trigger synthesis of carotenoids, which protect cells against photooxidative damage (Ortiz-Guerrero et al. 2011; Pérez-Marín et al. 2008; Takano et al. 2011).

CarH and TtCarH have a similar two-domain architecture. Both contain an N-terminal module similar to the MerR-type winged-helix DNA-binding domain of CarA, a *M. xanthus* CarH paralog (León et al. 2010; Navarro-Avilés et al. 2007; Pérez-Marín et al. 2008). CarH and TtCarH, as well as CarA, also possess a C-terminal domain with a B_{12}-binding motif of the type found in enzymes such as methionine synthase (Cervantes and Murillo 2002; Drennan et al. 1994; Ludwig and Matthews 1997; Ortiz-Guerrero et al. 2011; Pérez-Marín et al. 2008). CarH and CarA bind to the same operator DNA to regulate expression from a photoinducible promoter in *M. xanthus*. Despite their similar structural and functional domains, a striking difference between the two proteins is that CarH, but not CarA, absolutely requires B_{12} for activity (Ortiz-Guerrero et al. 2011; Pérez-Marín et al. 2008). We have shown that, of the two functional forms of B_{12} that exist in vivo, i.e., methylcobalamin (MeB_{12}) and 5′-deoxyadenosylcobalamin ($AdoB_{12}$) (Ludwig and Matthews 1997; Warren et al. 2002), it is $AdoB_{12}$ that is specifically required by CarH (Ortiz-Guerrero et al. 2011). Our analysis in vivo and in vitro demonstrated that $AdoB_{12}$-binding in the dark foments CarH or TtCarH oligomerization to enhance operator binding and block transcription; visible light (in the blue/green wavelength range where $AdoB_{12}$ absorbs) photolyzes bound $AdoB_{12}$, disrupts active repressor oligomers, weakens operator binding, and allows transcription (Ortiz-Guerrero et al. 2011).

Self-assembly, interaction with DNA, and the light dependence of CarH and TtCarH are thus intimately linked to $AdoB_{12}$ binding. Hence, in-depth characterization of these properties can provide valuable insights into the molecular mechanisms underlying photosensory gene regulation by these $AdoB_{12}$-dependent transcriptional factors. Toward this end, this study employs analytical ultracentrifugation (AUC) with sedimentation equilibrium (SE) as well as sedimentation velocity (SV) to examine $AdoB_{12}$-mediated oligomerization of TtCarH and its binding to DNA in the dark and in the light. Such studies with CarH, however, have been impeded by the inability to purify the native protein, in contrast to TtCarH. Another issue, given the photosensitivity of the $AdoB_{12}$-bound protein and its functional consequences, is that techniques such as AUC use light-based methods for detection and monitoring. To address this, we carried out several AUC experiments in interference optical mode under red light (655 nm, where $AdoB_{12}$ neither absorbs nor is photolyzed) and in absorbance optical mode using light that $AdoB_{12}$ absorbs [ultraviolet (UV) or visible blue/green range]. This combined approach has been used to probe the oligomerization state and overall shape of some other photoreceptors by AUC in earlier reports (Jurk et al. 2010; Zoltowski and Crane 2008). We obtained comparable results with both detection modes, indicating that either is applicable for studies of such proteins by AUC. Our data, supplemented with those from size-exclusion chromatography (SEC) and in vitro DNA-binding assays, demonstrate that $AdoB_{12}$-bound TtCarH is a tetramer in the dark with tight operator DNA-binding. On the other hand, apo and light-exposed $AdoB_{12}$-bound TtCarH are predominantly monomers with weak DNA-binding capability. Other oligomeric forms were either absent or present at negligible levels in the dark or in the light.

In addition to the insight provided by AUC into the light-dependent quaternary structure of a protein and its association to DNA, the present study demonstrates the feasibility of using AUC for light-dependent systems. Since the tertiary structure of the protein is as yet unknown, interpreting its hydrodynamic properties in terms of atomic- or residue-level modeling (Ortega et al. 2011) is not applicable. In such instances, the simple whole-modeling approach (Garcia de la Torre and Harding 2013; Harding 1995), based on classical principles and simple ellipsoidal models for biomolecular hydrodynamics, continues to be useful for evaluation of the gross conformation of proteins (e.g., folded and rigid versus unfolded and flexible, quasispherical versus elongated shapes, etc.; Ang et al. 2010), and has been applied with TtCarH. However, when dealing with more complex structures, such as that of the essentially rod-like DNA bound to the more globular TtCarH tetramer, the multisubunit HYDROSUB scheme (Garcia de la Torre and Carrasco 2002; Garcia de la Torre and Harding 2013) is found to have good predictive capability.

Materials and methods

Protein and DNA sample preparation

Cobalamins were obtained from Sigma-Aldrich, and preparation and concentration determinations of stock solutions were carried out as described previously (Ortiz-Guerrero et al. 2011). *Escherichia coli* strains DH5α and BL21-DE3 were used for plasmid constructions and protein overexpression, respectively. We have previously described (Ortiz-Guerrero et al. 2011) the pET15b plasmid construct to overexpress His_6-tagged TtCarH from the T7 promoter (Novagen) and protocols for its purification. Briefly, *E. coli* BL21(DE3) freshly transformed with the pET15b-*TtcarH* construct was grown in 10 ml Luria Broth LB medium and 100 μg/ml ampicillin (Amp) at 37 °C to optical density at 600 nm (OD_{600}) of 0.6–1.0. The 10-ml culture was then added to 1 l of fresh LB/Amp medium, grown to OD_{600} of 0.6–1.0 at 37 °C, at which time 0.5 mM isopropyl β-D-thiogalactoside (IPTG) was added to induce H_6-TtCarH

overexpression overnight at 25 °C. Cells were pelleted by centrifugation, and H_6-TtCarH was purified from the pellet under native conditions using TALON metal affinity resin and protocols (Clontech) with imidazole elution. Fractions containing purified protein were purified by size-exclusion chromatography (SEC) using a Superdex200 high-performance liquid chromatography (HPLC) column (GE Biosciences) equilibrated with 150 mM NaCl, 50 mM phosphate buffer, pH 7.5, and concentrated using Amicon Ultra (MWCO 3000Da). For purifying $AdoB_{12}$-H_6TtCarH, an ~fivefold excess of $AdoB_{12}$ was mixed with the apoprotein prior to SEC, and the $AdoB_{12}$-bound holoprotein was identified by absorbance at 360 and 522 nm as well as at 280 nm. Concentrations of stocks in aqueous buffer were determined using absorbance at 522 nm for $AdoB_{12}$ (ε_{522} = 8,200 M/cm), at 280 nm (ε_{280} = 37930/M/cm) for apo-H_6TtCarH, or the BioRad protein assay kit for apo- or holo-H_6TtCarH. The 177-bp DNA upstream of the *TtcarH* gene containing its promoter-operator regions was polymerase chain reaction (PCR)-amplified and purified using electrophoresis (1 % low-melting agarose) and the High Pure PCR purification kit (Roche). It was lyophilized and, when required, suspended in the desired buffer. DNA concentrations were estimated from the absorbance at 260 nm (ε_{260} = 2808951.9/M/cm or 2.5678/g/cm for a calculated molecular weight of 109,414.8 Da; http://biophysics.idtdna.com/UVSpectrum.html).

Light irradiation

Protein samples in 1.5-ml tubes were irradiated for 1–5 min with white light from three 18-W fluorescent lamps at intensity of approximately 10 W/m^2. For irradiation with light at specific wavelengths (405 and 465 nm in the blue–violet range, 520 nm in the green, and 660 nm in the red), for defined time periods, and with regulatable light intensities in the 0–20 W/m^2 range, we used a 5 × 5 cm^2 plate with 144 light-emitting diodes (LEDs) (arranged in 12 sectors, each with 12 LEDs in a 3 × 4 array; Cetoni GmbH, Germany) linked to a computer control center. Light intensities were estimated by using an 1815-C optical power meter equipped with an 818-SL detector (Newport).

Size-exclusion chromatography (SEC)

Size-exclusion chromatography was carried out in an AKTA HPLC unit using a Superdex200 analytical column (GE Life Sciences) equilibrated with 150 mM NaCl, 50 mM phosphate buffer, pH 7.5. The column calibration curve, obtained as described previously (Ortiz-Guerrero et al. 2011), was: $\log M_r = 7.885 - 0.221V_e$, where M_r is the apparent molecular weight and V_e is the elution volume. Protein (500 µl for purification, or 100 µl and 45–165 µM for analytical runs), pure or incubated with fivefold molar excess of $AdoB_{12}$ for at least 15 min in the dark, was injected into the column or subjected to light irradiation (when required) just prior to injection. Elution was carried out at flow rate of 0.3 or 0.4 ml/min and tracked using absorbance at 280, 361, and 522 nm. Peak fractions were collected, a 10–20-µl aliquot checked by sodium dodecyl sulfate-polyacrylamide gel electrophoresis (SDS-PAGE), and M_r was estimated from V_e. The reported value and error are the mean and standard error for three independent measurements.

DNA-binding assays

Electrophoretic mobility shift assays (EMSA) were performed in the dark or after light irradiation (as described earlier) using a 5′-end ^{32}P-labeled PCR-amplified 177-bp DNA probe. A 20-µl reaction volume containing the DNA probe (1.2 nM, approximately 13,000 cpm), protein with and without $AdoB_{12}$ at the required final concentrations (as indicated) in 100 mM KCl, 25 mM Tris, pH 8, 1 mM dithiothreitol (DTT), 10 % glycerol, 200 ng/µl bovine serum albumin (BSA), and 1 µg of sheared salmon sperm DNA as nonspecific competitor was incubated at 37 °C for 30 min in the dark and by covering samples with aluminum foil. Gel-loading and the EMSA runs were performed in a dark room under dim stray light (to aid viewing) and in a cooled chamber for 1.5 h at 200 V, 10 °C using a 6 % nondenaturing polyacrylamide gel (37.5:1 acrylamide:bisacrylamide) prerun for 30 min in 0.5× TBE buffer [45 mM Tris base, 45 mM boric acid, 1 mM ethylenediaminetetraacetic acid (EDTA)]. Gels were vacuum-dried and analyzed by autoradiography.

Analytical ultracentrifugation (AUC)

Analytical ultracentrifugation experiments were performed in a Beckman Coulter Optima XL-I analytical ultracentrifuge (Beckman-Coulter, Palo Alto, CA, USA) equipped with UV–visible absorbance as well as interference optical detection systems, using an An50Ti eight-hole rotor, 12-mm path-length charcoal-filled Epon double-sector centrepieces. The experiments were carried out at 20 °C (unless otherwise indicated) using samples in 150 mM NaCl, 50 mM sodium phosphate buffer at pH 7.5. Sample concentrations used ranged from 8 µM to 160 µM for H_6TtCarH protein and 0.05, 0.1, and 0.2 µM for DNA. AUC experiments were repeated at least twice, and the samples were checked by SDS-PAGE prior to and after the AUC experiment. Protein solutions and AUC cells were handled in the dark, but exposed to defined conditions under light when required as described earlier. Laser delay was adjusted prior to the runs to obtain high-quality

interference fringes. Light at wavelength of 655 nm was used in the interference optical mode, and at 260, 280 or 522 nm (unless otherwise stated) in the absorbance optical mode.

Sedimentation velocity (SV) runs were carried out at rotor speed of 45,000 rpm using 400-µl samples with the buffer used in the HPLC purification as reference. A series of 300 scans without time intervals between successive scans were acquired for each sample. Least-squares boundary modeling of the SV data was used to calculate sedimentation coefficient distributions using the size distribution $c(s)$ method (Schuck 2000) implemented in SEDFIT v11.71 software. Buffer density ($\rho = 1.0099$ g/ml) and viscosity ($\eta = 0.0103$ Poise) at 20 °C were calculated from the buffer composition and the partial specific volume of TtCarH using SEDNTERP software (Laue et al. 1992). The partial specific volumes used were 0.739 ml/g for TtCarH, as calculated from its amino acid sequence, and 0.55 ml/g for the 177-bp DNA, the standard literature value estimated for nucleic acids (Cohen and Eisenberg 1968). The molecular mass for TtCarH (from mass spectrometry or calculated from the amino acid sequence with the N-terminal Met processed out) was 33,141.03 Da, while that calculated for the DNA fragment was 109,414.8 Da. The diffusion coefficient (D) was extracted from the sedimentation profiles via the Lamm equation solution included in the $c(s)$ model of SEDFIT (Schuck 2000). The best fit values obtained for the sedimentation coefficient (s, in S or Svedbergs) and diffusion were used to estimate the molar mass of the molecule using the Svedberg equation

$$M = \frac{sRT}{D(1-\bar{v}\rho)}, \tag{1}$$

where $\bar{v}$ is the partial specific volume, ρ is the buffer density, T is the temperature, and R is the gas constant. The anhydrous frictional coefficient ratio f/f_0, where f is the frictional coefficient of the macromolecule and f_0 is the frictional coefficient of a sphere having the same molecular mass and specific volume as the macromolecule, measures the maximum shape asymmetry of the protein. We evaluated f/f_0 based on the relationship $s_{\text{sphere}}/s_{20,\text{w}} = f/f_0$, where s_{sphere} is the theoretical sedimentation coefficient of a sphere with the same molecular weight (M) and partial specific volume ($\bar{v}$) as the particle, obtained using

$$S_{\text{sphere}} = \frac{M(1-\bar{v}\rho)}{N_{\text{A}} 6\pi\eta\left(\frac{3M\bar{v}}{4\pi N_{\text{A}}}\right)^{\frac{1}{3}}}. \tag{2}$$

Here, η is the viscosity and N_{A} is Avogadro's number, and $s_{20,\text{w}}$ is the experimental s-value corrected to a standard state of water at 20 °C and infinite dilution as determined using SEDNTERP (Lebowitz et al. 2002). It should be noted that s_{sphere} would correspond to the maximum possible s-value for a particle of given molecular mass, since the surface area in contact with solvent would be minimum for a sphere and hence the frictional coefficient, f_0, would be minimum for that particle. Typical values of f/f_0 are 1.2–1.3 for globular proteins, 1.5–1.8 for elongated asymmetric proteins, and larger values for very elongated, cylindrical or unfolded proteins. The value of f/f_0 directly obtained from experimental data contains contributions due to protein shape and size expansion due to hydration. These two contributions can be factored in the form

$$\frac{f}{f_0} = P\left(1 + \frac{\delta}{\bar{v}\rho}\right)^{\frac{1}{3}}. \tag{3}$$

In the second term in the right-hand side of Eq. 3, δ is the hydration in grams of water per gram of macromolecule, which is commonly set to the consensus value of 0.3 g/g for proteins (Lebowitz et al. 2002) and 0.55 g/g for double-stranded DNA (Bastos et al. 2004). Then, P, the so-called Perrin function, measures the shape anisotropy of the particle, and in terms of the simple revolution-ellipsoid model, it is a function, $P(p)$, of the axial ratio p, with $p > 1$ for prolate ellipsoids and $p < 1$ for oblate ones. There is a large amount of evidence that most proteins tend to be prolate in shape, so this case is considered in the discussion of the results. For the above-mentioned evaluations, one must use an infinite-dilution sedimentation coefficient, $s^0_{20,\text{w}}$, which is obtained by extrapolation to zero concentration. We anticipate that in all our results the concentration dependence will be very weak (indicating dilute solutions very near the ideal limit), with $s_{20,\text{w}}$ nearly constant, so that small observed changes in $s_{20,\text{w}}$ with concentration essentially reflect experimental uncertainty and $s^0_{20,\text{w}}$ can be simply obtained as the mean value. This value is the one used in the evaluation of P. A departure of P from the value of 1 expected for a spherical particle provides an estimate of the shape anisotropy, which can be expressed in terms of the axial ratio, p, of the equivalent ellipsoid. We note, however, that while the determination of P includes uncertainties in the various terms in Eqs. 1–3, the $P(p)$ function deviates quite slowly from the limit for the spherical shape, $P(1) = 1$. Consequently, the deduced values of p must be considered only as rough estimates of shape.

Sedimentation equilibrium (SE) data were acquired for 180-µl samples at three different rotor speeds (as indicated in the text) in the absorbance and interference modes starting with the lowest and finishing with the highest rotor speed. At each speed, samples were sedimented to equilibrium, when successive scans at 6-h intervals were superimposable. The SE data were fit using SEDPHAT v6.21 software (Vistica et al. 2004) with the "single

species" or the "single species of interacting system" models to obtain the buoyant molecular weight corrected for the buoyancy factor by the partial specific volume calculated by SEDNTERP. Hydrodynamic properties of the DNA-TtCarH complexes were calculated using HYDROSUB (Garcia de la Torre and Carrasco 2002).

Results

SEC analysis of light-dependent, $AdoB_{12}$-driven TtCarH oligomerization

Size-exclusion chromatography analysis has revealed that the TtCarH C-terminal domain is a monomer in the dark or light and, in the presence of excess $AdoB_{12}$, a tetramer with 1:1 protein:$AdoB_{12}$ stoichiometry in the dark that yields a B_{12}-bound monomer in the light (Ortiz-Guerrero et al. 2011). Furthermore, the visible absorbance spectrum of the $AdoB_{12}$-bound tetramer resembles that of aqueous $AdoB_{12}$ solutions in the dark, whereas the spectrum of monomer generated in the light is similar to that of OHB_{12}, which is produced on $AdoB_{12}$ photolysis (Schwartz and Frey 2007). SEC profiles obtained in this study for full-length native TtCarH indicate a similar behavior (Fig. 1). Thus, apo-TtCarH elutes as a monomer with an apparent molecular weight (M_r) of 36.5 ± 0.8 kDa, close to the value of 33.14 kDa calculated from the monomer sequence or determined by mass spectrometry, whereas higher-molecular-weight species are undetected. By comparison, $AdoB_{12}$-bound holo-TtCarH in the dark elutes as a significantly larger species that absorbs at 280 and 522 nm and whose M_r of 136 ± 2 kDa is comparable to the value calculated (138 kDa) for an $AdoB_{12}$–TtCarH tetramer. Exposing the latter to green (522 nm) or white light yields a B_{12}-bound monomer ($M_r = 39 \pm 0.1$ kDa) with near-complete absence of the tetrameric form. On the other hand, apo-TtCarH with excess OHB_{12} present continues to elute as a monomer with $M_r = (40 \pm 2$ kDa) that absorbs at 361 or 522 nm, besides 280 nm, consistent with the presence of bound OHB_{12} (Fig. 1). Thus, apo-TtCarH, light-irradiated $AdoB_{12}$-bound holo-TtCarH, or apo-TtCarH in the presence of excess OHB_{12} all appear to be monomers, whereas $AdoB_{12}$-bound holo-TtCarH is a tetramer in the dark.

EMSA analysis of TtCarH-DNA binding

Gel-shift (EMSA) assays had previously indicated very low-affinity binding of apo-TtCarH to a 177-bp DNA probe containing its operator, with most of the DNA probe remaining free even at concentrations as high as 800 nM (Fig. 2a, b, lanes 2–5) (Ortiz-Guerrero et al. 2011). By contrast, a fivefold excess of $AdoB_{12}$ relative to protein

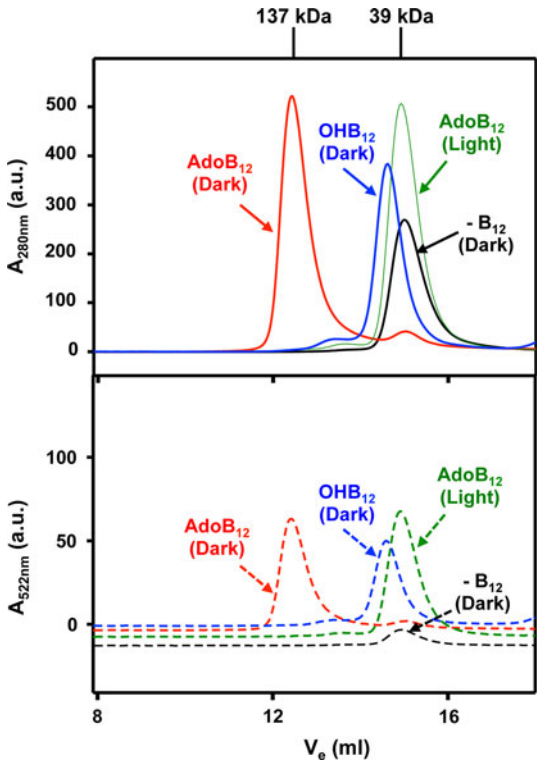

Fig. 1 Effects of $AdoB_{12}$ and light on TtCarH oligomerization analyzed using SEC. Elution profiles off a Superdex200 analytical SEC column tracked by the absorbance (in arbitrary units) at 280 nm (*top*, *solid lines*) or 522 nm (*bottom*, *dashed lines*) for 100 μM apo-TtCarH alone (*black lines*), for $AdoB_{12}$–TtCarH holoprotein in the dark (*red lines*) or after 5-min exposure to light at 522 nm (*green lines*), and for OHB_{12} added at fivefold excess relative to protein (*blue lines*). M_r (in kDa) is marked at the top for the two peak maxima corresponding to $AdoB_{12}$–TtCarH in the dark and in the light

was shown to markedly enhance DNA binding, with free probe being detected at very low levels for TtCarH concentrations ≥80 nM (lane 13, Fig. 2a; lanes 10–13, Fig. 2b) (Ortiz-Guerrero et al. 2011). However, this has not been previously examined with the $AdoB_{12}$–TtCarH holoprotein, in which $AdoB_{12}$ is present at stoichiometric levels relative to protein (1:1), the form employed in AUC analysis below. Our analysis with this $AdoB_{12}$–TtCarH holoprotein shows that the DNA probe was almost completely bound even at the lowest protein concentration examined of 10 nM (lanes 6–9; Fig. 2a), with any free DNA probe detected at very low levels at higher protein concentrations (lanes 6–9; Fig. 2b). Visible light at specified wavelengths produced similar effects on DNA binding by $AdoB_{12}$–TtCarH holoprotein as was observed with apo-TtCarH in the presence of fivefold excess of $AdoB_{12}$ (Fig. 2c). In either case, the complex corresponding to the well-defined retarded band formed in the dark at 200 nM protein concentration was disrupted by light in the blue–green range (405, 465, or 520 nm) but not by red light (655 nm), and consequently most of the DNA occurs as

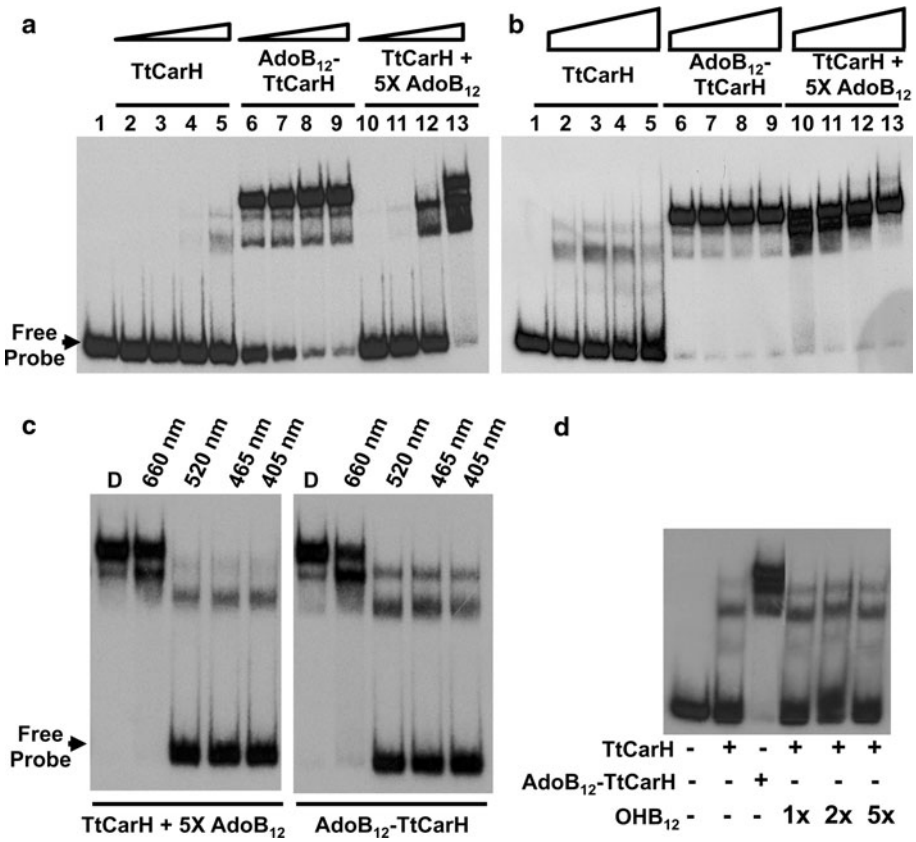

Fig. 2 DNA binding by $AdoB_{12}$–TtCarH holoprotein in the dark or light compared with apo-TtCarH alone, or with excess $AdoB_{12}$ or OHB_{12} present. **a** EMSA of the binding in the dark of the 177-bp DNA probe containing the TtCarH operator to apo-TtCarH (*lanes 2–5*), $AdoB_{12}$–TtCarH (*lanes 6–9*), and apo-TtCarH with fivefold molar excess of added $AdoB_{12}$ (*lanes 10–13*), as indicated. Protein concentrations (in nM) increase in the order 10, 20, 40, and 80. **b** Same as in (**a**) but with protein concentrations (in nM) increasing in the order 100, 200, 400, and 800. (**c**) EMSA of the binding to the DNA probe (as in **a** and **b**) of $AdoB_{12}$–TtCarH holoprotein (200 nM), or of apo-TtCarH (200 nM) in the presence of fivefold molar excess of $AdoB_{12}$ in the dark ("D") for 35 min, or after irradiation with light at the wavelengths (in nm) indicated at the top for 5 min after 30-min incubation in the dark. **d** EMSA as in **b** carried out in the dark for apo-TtCarH alone, $AdoB_{12}$–TtCarH holoprotein, or apo-TtCarH with equal, two-, or fivefold excess of OHB_{12} for samples containing 400 nM protein and in the dark

free probe (Fig. 2c). Only the weak binding that was also observed with apo-TtCarH (Fig. 2a, b) remained, as indicated by the two retarded bands of low intensity and greater mobilities. Since $AdoB_{12}$ is photolyzed to OHB_{12}, we checked the effect of adding excess OHB_{12} on DNA-binding by apo-TtCarH. This indicated weak DNA-binding similar to that observed for apo-TtCarH or for light-exposed $AdoB_{12}$–TtCarH holoprotein (Fig. 2d). Thus, whereas $AdoB_{12}$–TtCarH holoprotein binds to DNA with high affinity in the dark or under red light, exposure to blue–green light, which causes $AdoB_{12}$ photolysis, correlates with loss of DNA-binding.

AUC analyses indicate apo-TtCarH and light-exposed $AdoB_{12}$–TtCarH holoprotein to be monomers

The sedimentation coefficient obtained by direct fitting of the SV profiles can detect the presence of diverse components in the sample over a wide size range, and inform on the overall conformation, size, and shape of the macromolecule under study. A major advantage of this technique is that it avoids complications resulting from any interactions with the matrix or surfaces (as can occur in SEC or gel electrophoretic methods such as EMSA) and provides details on each component within the sample. We analyzed SV data in both absorbance and interference optical modes for apo-TtCarH at three different concentrations: 30, 15, and 8 μM.

In all these cases, analysis of the SV experimental data using the size distribution $c(s)$ method implemented in SEDFIT (see "Materials and methods" section) yielded a well-defined, single peak. Also, the quality of the fit, as can be deduced from the plot of residuals (Fig. 3a), is quite good. The peak positions provide sedimentation coefficients which, as anticipated above and within experimental uncertainties, are concentration independent, and a mean

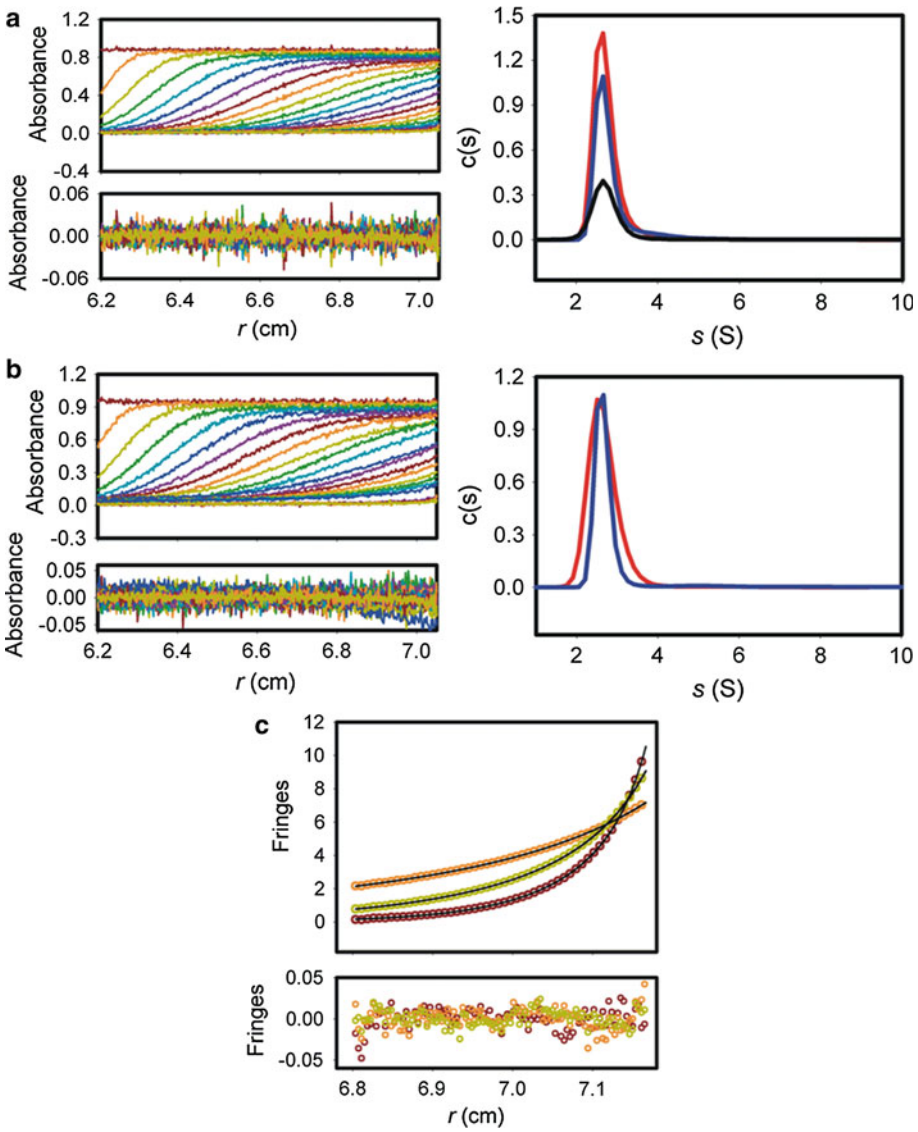

Fig. 3 AUC analysis of apo-TtCarH and light-exposed $AdoB_{12}$–TtCarH holoprotein. **a** SV analysis of apo-TtCarH. *Left panels*: raw SV profiles recorded using absorbance at 280 nm for 30 μM apo-TtCarH at 45,000 rpm, 20 °C, and different times (*top*), and residuals for the best fit to the continuous sedimentation coefficient distribution $c(s)$ model (*bottom*). *Right panel*: sedimentation coefficient $c(s)$ distributions for 30 μM (*red*), 15 μM (*blue*) or 8 μM (*black*) apo-TtCarH. **b** SV analysis of light-exposed $AdoB_{12}$–TtCarH. *Left panels*: raw SV profiles for 40 μM light-exposed $AdoB_{12}$–TtCarH acquired using absorbance at 280 nm, 45,000 rpm, 20 °C, and different times (*top*), and residuals for the best $c(s)$ model fits (*bottom*). *Right panel*: sedimentation coefficient $c(s)$ distributions for 40 μM (*red*) and 10 μM (*blue*) of $AdoB_{12}$–TtCarH (*right*). **c** SE analysis of apo-TtCarH. SE gradients recorded using interference (655 nm) for 22 μM apo-TtCarH at 20 °C, and at 10,000 rpm (*orange circles*), 15,000 rpm (*green circles*) or 20,000 rpm (*purple circles*), the lines through the data representing the best fit using the SEDPHAT discrete species model for two species, with residuals for the fit shown below

$s^0_{20,w}$ of 2.59 ± 0.04 S corresponds to this form of the protein. Furthermore, the quality of the fitting of the AUC concentration profiles allows a reliable estimate of the diffusion coefficient (D) to be extracted from the sedimentation profiles using the Lamm equation solution included in the $c(s)$ model of SEDFIT. From this we estimated a molecular weight of 32.1 ± 0.8 kDa, in concordance with the calculated monomer molecular weight of 33.14 kDa for TtCarH. Results are listed in Table 1. Using the values of M and $s^0_{20,w}$ in Eqs. 2 and 3, with hydration of $\delta = 0.3$ g/g, the value of the shape-dependent Perrin function is $P = 1.11$.

Next, we carried out a similar SV analysis with light-exposed $AdoB_{12}$–TtCarH (which mirrors apo-TtCarH in being a monomer and in weak DNA-binding according to size-exclusion and EMSA analyses) at concentrations of 160, 40, and 15 μM. Overall, the peak positions as well as the numerical values were very similar to those obtained

for apo-TtCarH. The (nearly concentration-independent) sedimentation coefficients, from both absorbance and interference experiments (Fig. 3b; Table 1), reduce to $s^0_{20,w} = 2.64$ S. Again, as with apo-TtCarH, the fits of the sedimentation profile were very good, yielding a molecular weight estimate of approximately 31.5 ± 0.7 kDa, indicating that the species present in the solution at these concentrations is predominantly monomeric, while the shape analysis yielded $P = 1.15$.

The general conclusion from these two sets of SV experiments is that the two forms, i.e., apo-TtCarH and light-exposed $AdoB_{12}$–TtCarH, are largely identical in AUC, with nearly the same molecular mass (any contribution from the ligand being relatively minor). The protein

Table 1 Summary of the analysis of analytical ultracentrifugation data

Sample	Conc. (μM)	SV ($\bar{s}_{20,w}$)		SE	
		Abs	Int	Conc. (μM)	M (kDa)
Apo-TtCarH	30	2.60	2.59	30	32.6 ± 0.3
	15	2.57	2.58	22	
	8	2.58	2.62		
	0	$s^0_{20,w} = 2.59$			
		$P = 1.11$	$p \approx 3.0$		
$AdoB_{12}$–TtCarH (light)	160	2.56 ± 0.14	–	50	30 ± 3
	40	2.63 ± 0.13	2.76	38	
	10	2.61 ± 0.12	2.68		
	0	$s^0_{20,w} = 2.64$			
		$P = 1.15$	$p \approx 3.5$		
$AdoB_{12}$–TtCarH (dark)	160*	6.39	6.24	50[c], 40[c]	122 ± 11[c]
	40*	6.34	6.21	20[c], 10[c]	
	10	6.31		125[d]	121 ± 14[c]
	0	$s^0_{20,w} = 6.25$		38[d]	
		$P = 1.16$	$p \approx 3.7$		
DNA	0.1	5.19	–		112 ± 6
	0.2	5.16	–		
		Rod model, predicted: $s^0_{20,w} = 5.3$			
Apo-TtCarH + DNA	10[a]	2.31	2.29		
	0.05[b]	4.40	4.50		
		6.87	6.83		
		(See text)			
$AdoB_{12}$–TtCarH + DNA (light)	10[a]	2.47	2.46		
	0.1[b]	4.67	4.80		
		6.43	6.49		
		(See text)			
$AdoB_{12}$–TtCarH + DNA (dark)	10[a]	6.11[f]			
	0.1[b]	7.90[g]			
		11.0			
		HYDROSUB: $s^0_{20,w} = 8.0$			

* 10 % of species with $\bar{s}_{20,w} = 9.4$

[a] TtCarH

[b] DNA

[c] Interference mode

[d] Absorbance mode

[f] Assigned to free $AdoB_{12}$–TtCarH

[g] Assigned to $AdoB_{12}$–TtCarH + DNA complex

shape, with $P = 1.11$–1.15, in terms of a prolate ellipsoid would correspond to an axial ratio of $p = 3.0$–3.5 from which, notwithstanding the associated uncertainties noted earlier, it may be reasonable to conclude that the TtCarH monomer forms are appreciably elongated.

As mentioned earlier, SV data were acquired by monitoring absorbance at 280 nm or visible light at wavelengths at which $AdoB_{12}$ does absorb and, for comparison, independently using interference optics and a wavelength (655 nm) corresponding to red light, at which $AdoB_{12}$ does not absorb. This was done to check for any effects of light absorbance at the laser intensities required for detection in the AUC experiments, given the photosensitivity of $AdoB_{12}$, and is particularly relevant for the analysis carried out in the dark as will be described in the next section. For apo-TtCarH or light-exposed $AdoB_{12}$–TtCarH, we found that SV data obtained in absorbance versus interference mode yielded reproducible sedimentation coefficient distributions (data not shown), indicating the absence of any light-dependent effects and the suitability of both detection modes for AUC analysis.

Sedimentation equilibrium analyses were carried out at various speeds to directly estimate the buoyant molecular weight of apo-TtCarH at 30 and 22 μM, and of light-exposed $AdoB_{12}$–TtCarH at 50 and 38 μM. Figure 3c shows representative SE data obtained for apo-TtCarH at 22 μM at different speeds. The average molecular weight calculated from a global fit of the SE concentration profiles at the three speeds was 32.6 ± 0.3 kDa for TtCarH and 30 ± 3 kDa for light-exposed $AdoB_{12}$–TtCarH (Table 1), very similar to estimates from SV data or calculated from the sequence for a monomer.

AUC analyses indicate $AdoB_{12}$–TtCarH holoprotein to be a tetramer in the dark

The oligomeric nature, DNA-binding, and in vivo function of $AdoB_{12}$–TtCarH in the dark are, as mentioned earlier, dramatically altered on exposure to light. We therefore examined using AUC how $AdoB_{12}$–TtCarH in solution behaves in the dark, taking extreme care to carry out all sample manipulation, cell loading, and alignment (in the rotor) under low-intensity red light (>650 nm), thereby avoiding sample exposure to light that could cause $AdoB_{12}$ photolysis and consequently affect $AdoB_{12}$–TtCarH oligomerization. SV or SE runs were monitored in the interference optical mode using red light (655 nm), and the results thus obtained were compared with those obtained using absorbance at 280 nm (where protein and $AdoB_{12}$ absorb) or at 522 nm (where only $AdoB_{12}$ absorbs). Samples, otherwise maintained in the dark, were exposed to light only during the time interval corresponding to detection. Data were also obtained at 260 nm, since this wavelength was used for samples that contained DNA in the next section.

SV data (Fig. 4a), recorded at three concentrations of $AdoB_{12}$–TtCarH of 160, 40, and 10 μM, and analyzed using the SEDFIT software for size distribution $c(s)$ analysis, were fit for a set of 150 equispaced values of the sedimentation coefficient over the range 0.1–15.0 S at 20 °C. One peak essentially around 6.2–6.4 S for the three protein concentrations (Table 1) dominated the $c(s)$ overlay, although minor peaks with higher sedimentation coefficients could be detected, but only at 160 μM, the highest $AdoB_{12}$–TtCarH concentration used. It is noteworthy that similar results were obtained from the data using absorbance at 522 nm (Fig. 4a), at which only $AdoB_{12}$ but not protein absorbs, as with those derived from the absorbance at 280 nm (not shown), at which the protein also absorbs. While signal intensities at the two wavelengths differ, consistent with the distinct absorption coefficients at each wavelength, the peak positions are identical.

Using a mean value of 6.25 S for $s^0_{20,w}$ and a molecular weight of 138 kDa expected for an $AdoB_{12}$-bound TtCarH tetramer based on the calculated monomer value of 34.5 kDa (as verified by the SE experiment), we carried out the analysis of the Perrin function as in the previous cases. The results are $f/f_0 = 1.30$ and $P = 1.16$, respectively. The shape anisotropy is thus close to that of the monomeric apo or light-exposed forms. Again, while little structural detail can be inferred from these data, it does appear that the tetramer is not more elongated than the monomer itself. From previous knowledge on the hydrodynamics of oligomers composed of elongated subunits (Lopez Martinez and Garcia de la Torre 1983), we suspect that a compact, side-by-side arrangement would be more likely than an elongated head-to-tail attachment.

The predominance of the same tetramer species over the range of concentrations studied (10–160 μM) also suggests the tendency of TtCarH to self-associate in the presence of $AdoB_{12}$ to form a stable tetramer. In sum, the principal peak in the sedimentation coefficient distribution and hence predominant form observed in the 10–160 μM concentration range for $AdoB_{12}$–TtCarH in the dark is a tetramer, which is more compact and closer to a spherical form than either apo-TtCarH or light-exposed $AdoB_{12}$–TtCarH monomers.

To further characterize $AdoB_{12}$–TtCarH in the dark and to complement the SV data, we also carried out multispeed SE analysis in the interference mode in the dark at 20 °C and three speeds (10,000, 15,000, and 20,000 rpm) for protein concentrations of 125, 50, 40, 20, and 10 μM. Analysis of SE data (after a 6-day equilibrium run) fitted to a single or two species indicated a predominant one corresponding to 122 ± 11 kDa (Fig. 4b; Table 1). Analysis

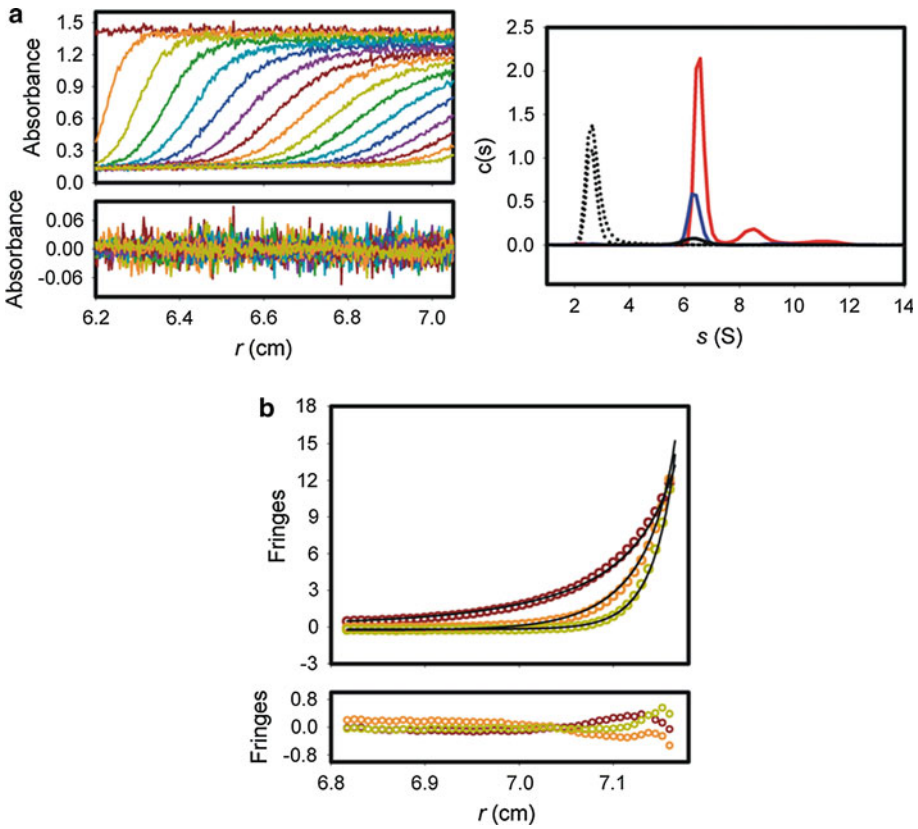

Fig. 4 AUC analysis of $AdoB_{12}$–TtCarH holoprotein. **a** *Left panel*: raw SV profiles for 40 μM $AdoB_{12}$–TtCarH recorded in the dark at 45,000 rpm, 20 °C, and different times using absorbance at 522 nm (*top*) and the residuals for the best *c*(*s*) model fit (*bottom*). *Right panel*: sedimentation coefficient distribution, *c*(*s*), for 160 μM (*red line*), 40 μM (*blue line*), and 10 μM (*black lines*) $AdoB_{12}$–TtCarH, with the *dotted lines* corresponding to data for 30 μM apo-TtCarH and 40 μM light-exposed $AdoB_{12}$–TtCarH from Fig. 3a and b shown for comparison. **b** SE analysis of 50 μM $AdoB_{12}$–TtCarH holoprotein. SE gradients in the dark recorded using interference (655 nm) and at 10,000 rpm (*purple circles*), 15,000 rpm (*orange circles*), and 20,000 rpm (*green circles*), the continuous line being the best fit to the SEDPHAT discrete species model for two species. Residuals for this fit are shown in the *bottom*

of SE data obtained in the absorbance mode at 280 or 522 nm and for protein concentrations of 40 and 10 μM again indicated a single species with molecular weight of 121 ± 14 kDa, similar to that from interference data at 655 nm. This suggests that the absorbance mode is suitable for AUC of the light-sensitive $AdoB_{12}$–TtCarH, otherwise maintained in the dark (Table 1). These molecular weight estimates from SE data obtained for $AdoB_{12}$–TtCarH in the dark are close to, but somewhat lower than, the calculated value for a tetramer or those estimated from SV data. A possible reason may be a tendency for the protein to degrade partially, which we found to occur occasionally during the long SE runs in a time-dependent manner, as inferred from SDS-PAGE analysis of AUC samples before and after an SE run. As a result, a stable fragment resistant to further degradation persisted, which N-terminal sequencing and mass spectrometry identified to be the TtCarH C-terminal B_{12}-binding domain. This domain can also form $AdoB_{12}$-bound tetramers in the dark (according to SEC; Ortiz-Guerrero et al. 2011), which could contribute to the lower than expected tetramer molecular weight estimated by the single-species fitting of SE data.

TtCarH binds to operator DNA in the dark as a tetramer

In the dark, $AdoB_{12}$–TtCarH is a tetramer and binds with maximum affinity to its operator as described above. Hence, we next examined using AUC the behavior of $AdoB_{12}$–TtCarH in solution when DNA containing the TtCarH operator sequence was also present in the dark as well as in the light. For this, we used the 177-bp DNA fragment that was used in the EMSA analysis of TtCarH-DNA binding (produced in sufficient amounts for AUC by PCR as described in the "Materials and methods" section). SV analysis was carried out in the absorbance mode at 258, 280, and 522 nm with 0.1 or 0.2 μM of this DNA, alone, in the presence of 10 μM $AdoB_{12}$–TtCarH in the dark or light-exposed, or of apo-TtCarH. For the sample with DNA alone, the sedimentation coefficient distribution *c*(*s*) model analysis was carried out with the data obtained at 258 or

280 nm (but not at 522 nm, where DNA does not absorb) using SEDFIT. The outcome indicated a single species at both 0.1 μM as well as 0.2 μM DNA, characterized by a narrow peak (Fig. 5a) corresponding to $s_{20,w}$ of 5.2 ± 0.1 S at both concentrations. For this 177-bp double-stranded DNA, the contour length, L, is about 60 nm and its ratio to the persistence length $a \approx 55$ nm is close to unity. Under these conditions (Ortega et al. 2011), DNA behaves like a fairly long but still rigid rod. An ellipsoidal model is invalid in such a case; rod-like DNA is customarily modeled as a cylinder. For DNA, the hydrodynamic radius is $d = 2.2$ nm, and the mass per unit length is $M_L = 1{,}950$ Da/nm (Ortega et al. 2011). For such values of d, L, a, and M_L, the theory of cylindrical particles (Ortega and Garcia de la Torre 2003) predicts a sedimentation coefficient of 5.3 S, which is in excellent agreement with our experimental data. Furthermore, the molecular weight estimate of 112 kDa obtained from our SV experiment agrees well with the expected value of 109,414.8 Da for the 177-bp DNA fragment.

Sedimentation velocity data analysis for samples containing DNA and $AdoB_{12}$–TtCarH and examined in the dark at 258, 280 or 522 nm presented a more complex profile: two main peaks are readily apparent at all three wavelengths used, corresponding to entities sedimenting at $s_{20,w} = 6.11$ S and $s_{20,w} = 7.90$ S; a minor peak corresponding to a third species with $s_{20,w} = 11.0$ S can also be discerned but at much lower levels.

For the prediction of the sedimentation coefficient of the protein–DNA complex, a more sophisticated, but still simple procedure is feasible with the program HYDROSUB (Garcia de la Torre and Carrasco 2002), which constructs models with cylindrical, ellipsoidal, and spherical subunits. The above dimensions of the cylinder were used for the rod-like DNA. As per the bound protein, considering the uncertainties in both its actual shape and in its mode of binding to DNA, the HYDROSUB prediction for the complex was performed considering the $AdoB_{12}$–TtCarH tetramer modeled as an equivalent sphere of radius 37.7 Å, calculated from the tetramer molecular weight together with $\delta = 0.3$ g/g hydration bound to a cylindrical DNA of 600 × 22 Å. HYDROSUB yielded a sedimentation coefficient of 8.00 S under standard conditions, close to the major $s_{20,w} = 7.90$ S species observed on analysis of SV data, suggesting that the latter is very likely a complex of $AdoB_{12}$–TtCarH tetramer bound to the 177-bp DNA. The second major peak corresponding to 6.1 S can be attributed to free $AdoB_{12}$–TtCarH tetramer, which has an essentially identical value (6.11 S) as described in the previous section, and is present in large excess over DNA. The species at 11.4 S is present at low, albeit detectable, levels, and its identity remains to be assigned. Probably, it is a higher-order $AdoB_{12}$–TtCarH oligomer that, we speculate, is DNA-bound rather than free protein because it is observed at 10 μM $AdoB_{12}$–TtCarH, and a similar species could not be detected at this low concentration of the protein alone (Fig. 4a).

SV analysis of samples containing 0.1 μM DNA and 10 μM $AdoB_{12}$–TtCarH exposed to light (Fig. 5c) revealed a major species with $s_{20,w} = 2.47$ S that would be the free protein unbound to DNA, since it closely matches the $s_{20,w}$ of $AdoB_{12}$–TtCarH alone (Fig. 3b; Table 1). A significantly populated species with $s_{20,w} = 6.43$ S and one present at very low levels with $s_{20,w} = 4.7$ S could also be detected. Neither of these were apparent in samples of DNA alone ($s_{20,w}$ of ~5.2) or of light-exposed $AdoB_{12}$–TtCarH alone. Their identities thus remain to be assigned. Their appearance only in a sample containing DNA together with excess light-exposed $AdoB_{12}$–TtCarH suggests that these may be protein–DNA complexes of sizes smaller than that of the one that the $AdoB_{12}$–TtCarH tetramer forms with DNA in the dark. The existence of a complex of smaller size is consistent with EMSA results of operator DNA-binding to $AdoB_{12}$–TtCarH exposed to light (where overall DNA-binding is weak) in which retarded bands are observed whose gel mobilities are faster than that of the tightly bound complex that $AdoB_{12}$–TtCarH forms in the dark (Fig. 2). Whereas EMSA indicated that of the presence of light-exposed $AdoB_{12}$–TtCarH most of the DNA probe remained free, we did not detect any species in the SV profile that could be assigned to free DNA. Possibly, the very large (100-fold) excess of protein over DNA depletes free DNA. The species at 6.4 S could therefore correspond to a DNA-bound complex of two light-exposed $AdoB_{12}$–TtCarH monomer(s) based on a HYDROSUB calculation where two $AdoB_{12}$–TtCarH monomers modeled as spheres of radius 24.2 Å bound to a cylindrical DNA showed a sedimentation coefficient of 6.49 S. SV analysis yielded similar results in solutions containing 0.1 μM DNA and 10 μM apo-TtCarH: a major species that can be assigned to free protein ($s_{20,w} = 2.31$ S); a second significantly populated species with $s_{20,w} = 6.87$ S that may be, as with light-exposed $AdoB_{12}$–TtCarH, a DNA-bound complex with two apo-TtCarH monomers; and a very minor species with $s_{20,w} = 4.4 \pm 0.2$ S. It has been pointed out elsewhere (see Schuck 2010a, b; Zhao et al. 2011) that the characteristics of the reaction boundary formed during the sedimentation of rapidly interacting species (as could be the case for the binding of apo or light-exposed TtCarH to DNA) and the less complex one of the individual partner in excess (here the protein) can be simulated to estimate the stoichiometry of the labile complex. This, however, cannot be ascertained based only on a single SV profile, as is the case here, and therefore the more sophisticated analysis of simulating the boundary characteristics was not attempted. In sum, AUC data

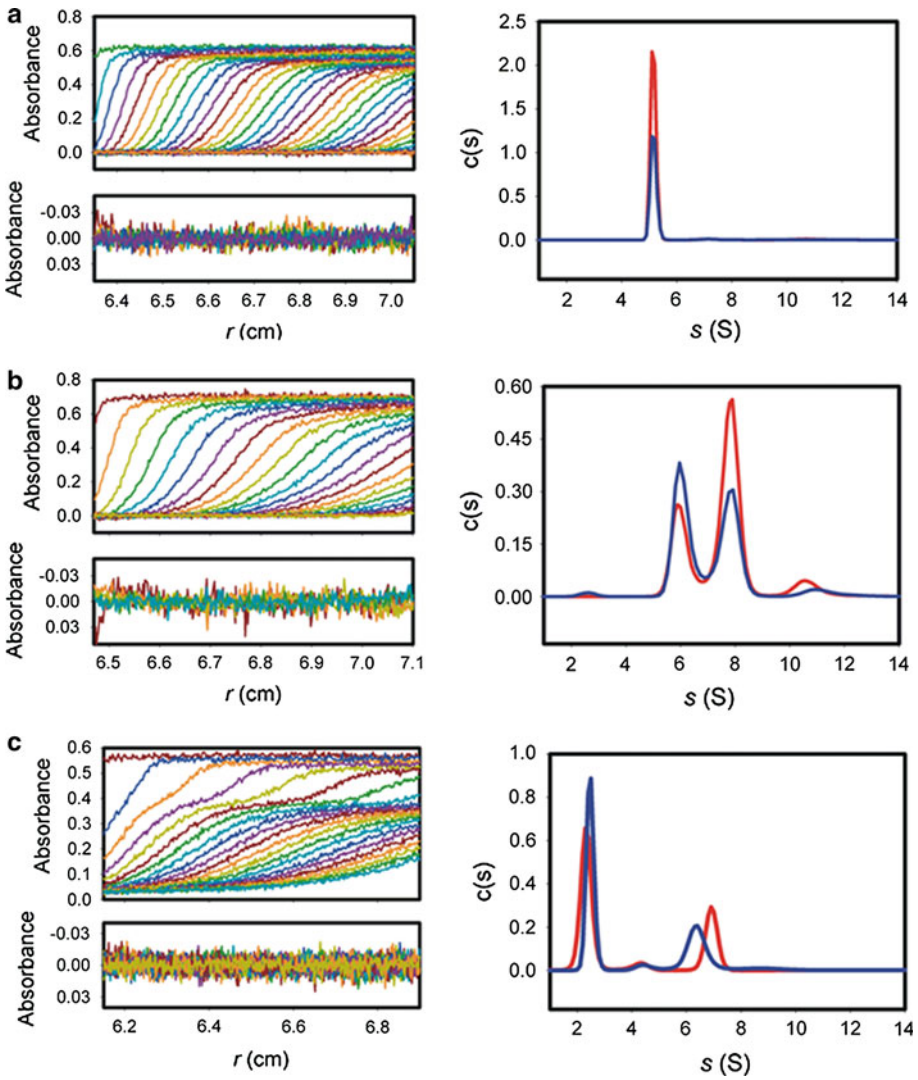

Fig. 5 AUC analysis of TtCarH in the presence of operator DNA. **a** SV analysis of the 177-bp DNA fragment containing the TtCarH operator. Raw SV profiles for 0.1 μM DNA at 45,000 rpm, 20 °C, and different times using absorbance at 260 nm (*top-left panel*), residuals for the best *c*(*s*) model fit (*bottom-left panel*), and sedimentation coefficient distribution, *c*(*s*) for 0.1 μM (*blue*) and 0.2 μM (*red*) DNA (*right panel*). **b** SV analysis in the dark of 0.1 μM 177-bp TtCarH operator DNA fragment with 10 μM $AdoB_{12}$–TtCarH present. Raw SV profiles obtained at 45,000 rpm, 20 °C, and different times using absorbance at 260 nm (*top-left panel*), residuals for the best *c*(*s*) model fit (*bottom-left panel*), and sedimentation coefficient distribution, *c*(*s*), from fits of the profiles obtained from the absorbance at 260 nm (in *red*) or at 280 nm (in *blue*) (*right panel*). **c** SV analysis in the dark of 0.1 μM 177-bp TtCarH operator DNA fragment with 10 μM $AdoB_{12}$–TtCarH present and exposed to light. Raw SV profiles obtained at 45,000 rpm, 20 °C, and different times using absorbance at 260 nm (*top-left panel*), residuals for the best *c*(*s*) model fit (*bottom-left panel*), and sedimentation coefficient distribution, *c*(*s*), from fits of the profiles obtained from the absorbance at 260 nm (in *red*) or at 280 nm (in *blue*) (*right panel*)

suggest that apo-TtCarH or light-exposed $AdoB_{12}$–TtCarH can bind to operator DNA but the complex formed is significantly smaller in size than that observed with $AdoB_{12}$–TtCarH tetramer in the dark, consistent with EMSA data.

Discussion

TtCarH is a transcriptional factor involved in regulating light-induced carotenogenesis in *T. thermophilus* (Takano et al. 2011). When its C-terminal domain (which contains a methionine synthase-type B_{12}-binding motif) is bound to $AdoB_{12}$, TtCarH is an oligomer that binds tightly to operator DNA via an N-terminal MerR-type DNA-binding domain. Photolysis of $AdoB_{12}$ leads to oligomer disruption and thereby to a dramatic decrease in DNA binding (Ortiz-Guerrero et al. 2011). The light-sensing regulatory action of $AdoB_{12}$–TtCarH is thus intimately linked to its oligomerization state, and knowledge of this is necessary to fully understand the molecular mechanisms underlying

TtCarH interactions and functions. In the present study, we examined using AUC methods apo-TtCarH as well as the $AdoB_{12}$-bound holo form in the dark and in the light, and in the absence and presence of operator DNA. Sedimentation coefficients obtained from SV data were interpreted based on hydrodynamic modeling, while SE data provided estimates of the buoyant molecular weight of the species.

Analytical ultracentrifugation data from SV and SE experiments indicate that apo-TtCarH and light-exposed holo $AdoB_{12}$–TtCarH at the concentrations examined exist in solution as monomers with higher-order oligomers essentially absent, and that both of these TtCarH monomeric forms are aspherical ellipsoids. On the other hand, $AdoB_{12}$–TtCarH holoprotein exists, when not exposed to light, almost entirely as a tetramer that is more spherical and compact. While low levels of larger oligomers possibly form at higher protein concentrations, monomers or dimers were undetected. Comparable results were obtained for $AdoB_{12}$–TtCarH self-association in the dark using AUC data acquired in the interference optical mode with wavelengths corresponding to red light or those using absorbance optics at wavelengths at which protein or $AdoB_{12}$ absorb. Thus, the duration and intensity of the laser pulse used for data acquisition in the absorbance mode do not cause significant photolysis of the light-sensitive $AdoB_{12}$–TtCarH, indicating that not only the interference mode but also the absorbance optical mode is applicable for AUC analysis of this protein. The use of both detection modes to examine light-sensitive proteins has been reported previously for some other photoreceptors such as in AUC studies of the oligomerization state and overall shape of the LOV family VIVID and YtvA proteins (Jurk et al. 2010; Zoltowski and Crane 2008). The oligomeric states of the apo and holo TtCarH forms in the presence or absence of light that we deduced from AUC analyses are also in overall agreement with findings from analytical gel filtration experiments, in which proteins are loaded at concentrations in the same range as used for AUC but are typically diluted during the course of elution.

Gel-shift assays indicate that $AdoB_{12}$–TtCarH binds tightly to operator DNA in the dark but in the light, or with apo-TtCarH, this DNA-binding is considerably weakened, with complexes of size smaller than that observed for $AdoB_{12}$–TtCarH in the dark being formed at low levels. Hydrodynamic modeling together with analysis of AUC data obtained for solutions containing operator DNA and 100-fold excess of $AdoB_{12}$–TtCarH suggest that in the dark essentially all of the DNA was bound as a complex with a tetramer of $AdoB_{12}$–TtCarH. A similar analysis of the $AdoB_{12}$–TtCarH-DNA complex but in the light, or with the apo form, indicated the formation of a complex of smaller size that may correspond to a complex of 2:1 $AdoB_{12}$–TtCarH:DNA stoichiometry, but this is speculative at this time and remains to be confirmed. These inferences from the AUC data obtained in the dark and in the light are thus in overall agreement with observations in gel-shift assays. Our AUC analysis indicates that DNA-binding by apo-TtCarH mirrors that observed for light-exposed $AdoB_{12}$–TtCarH.

In summary, our AUC experiments (with the added difficulty in dealing with a light-sensitive system), along with our hydrodynamic analysis (with either global-fitting ellipsoids or subunit models) provide insights into the light-dependent self-association and DNA-binding of TtCarH, which are in broad agreement with inferences based on analytical gel filtration and gel-shift DNA-binding assays. They show that, while $AdoB_{12}$–TtCarH is a compact tetramer in the dark, and a more ellipsoidal monomer when exposed to light or in the B_{12}-free apo form, other higher- or lower-order oligomeric forms are largely absent. It is also as a tetramer that $AdoB_{12}$–TtCarH appears to bind operator-containing DNA, but smaller complexes are observed for the weak DNA-binding of light-exposed $AdoB_{12}$–TtCarH or the apo form. Our study demonstrates that AUC can be employed to characterize such light-sensitive proteins, and sets the stage for future experiments aimed at elucidating binding constants, cooperativity, and other thermodynamic properties for this $AdoB_{12}$-dependent self-association and DNA-binding.

Acknowledgments We thank (from Universidad de Murcia) Dr. Alejandro Torrecillas for mass spectrometry analysis and J.A. Madrid for technical assistance. This work was funded by the Ministerio de Ciencia e Innovación (MICINN)-Spain and Ministerio de Economía y Competitividad (MINECO)-Spain grants to S.P. (BFU2009-12445-C02-02; BFU2012-40184-C02-02), to J.G.T. (CTQ-2009-08030; CTQ-2012-33717), and to M.E.-A. (BFU2009-12445-C02-01; BFU2012-40184-C02-01), the grants to J.G.T. and M.E.-A. co-financed by the European Union (FEDER). J.G.T also received funding from a Grupo de Excelencia de la Región de Murcia grant 04531/GERM/06. A.I.D. is the recipient of a FPI-MICINN grant. A.O. was supported by a postdoctoral fellowship from Fundación CajaMurcia, and J.M.O.-G. by a Consejo Superior de Investigaciones Científicas (Spain) JAE-Predoc fellowship.

References

Ang S, Kogulanathan J, Morris GA, Kok MS, Shewry PR, Tatham AS, Adams GG, Rowe AJ, Harding SE (2010) Structure and heterogeneity of gliadin: a hydrodynamic evaluation. Eur Biophys J 39:255–261

Banerjee R, Ragsdale SW (2003) The many faces of vitamin B_{12}: catalysis by cobalamin-dependent enzymes. Annu Rev Biochem 72:209–247

Bastos M, Castro V, Mrevlishvili G, Teixeira J (2004) Hydration of ds-DNA and ss-DNA by neutron quasielastic scattering. Biophys J 86:3822–3827

Cervantes M, Murillo FJ (2002) Role for vitamin B_{12} in light induction of gene expression in the bacterium *Myxococcus xanthus*. J Bacteriol 184:2215–2224

Cohen G, Eisenberg H (1968) Deoxyribonucleate solutions: sedimentation in a density gradient, partial specific volumes, density and refractive index increments, and preferential interactions. Biopolymers 6:1077–1100

Croft MT, Lawrence AD, Raux-Deery E, Warren MJ, Smith AG (2005) Algae acquire vitamin B_{12} through a symbiotic relationship with bacteria. Nature 438:90–93

Drennan CL, Huang S, Drummond JT, Matthews RG, Ludwig ML (1994) How a protein binds B_{12}: a 3.0 A X-ray structure of B_{12}-binding domains of methionine synthase. Science 266:1669–1674

Garcia de la Torre J, Carrasco B (2002) Hydrodynamic properties of rigid macromolecules composed of ellipsoidal and cylindrical subunits. Biopolymers 63:163–167

Garcia de la Torre J, Harding SE (2013) Hydrodynamic modelling of protein conformation in solution. Biophys Rev (to be published)

Harding SE (1995) On the hydrodynamic analysis of macromolecular conformation. Biophys Chem 55:69–93

Johnson JE Jr, Reyes FE, Polaski JT, Batey RT (2012) B_{12} cofactors directly stabilize an mRNA regulatory switch. Nature 492:133–137

Jurk M, Dorn M, Kikhney A, Svergun D, Gartner W, Schmieder P (2010) The switch that does not flip: the blue-light receptor YtvA from *Bacillus subtilis* adopts an elongated dimer conformation independent of the activation state as revealed by a combined AUC and SAXS study. J Mol Biol 403:78–87

Laue TM, Shah BD, Ridgeway TM, Pelletier SL (1992) Computer-aided interpretation of analytical sedimentation data for proteins. In: Harding SE, Rowe AJ, Horton JC (eds) Analytical ultracentrifugation in biochemistry and polymer science. Royal Society of Chemistry, Cambridge, UK, pp 90–125

Lebowitz J, Lewis MS, Schuck P (2002) Modern analytical ultracentrifugation in protein science: a tutorial review. Protein Sci 11:2067–2079

León E, Navarro-Avilés G, Santiveri CM, Flores-Flores C, Rico M, González C, Murillo FJ, Elías-Arnanz M, Jiménez MA, Padmanabhan S (2010) A bacterial antirepressor with SH3 domain topology mimics operator DNA in sequestering the repressor DNA recognition helix. Nucleic Acids Res 38:5226–5241

Lopez Martinez MC, Garcia de la Torre J (1983) Transport properties of rigid, symmetrical oligomeric structures composed of prolate, ellipsoidal subunits. Biophys Chem 18:269–279

Ludwig ML, Matthews RG (1997) Structure-based perspectives on B_{12}-dependent enzymes. Annu Rev Biochem 66:269–313

Nahvi A, Sudarsan N, Ebert MS, Zou X, Brown KL, Breaker RR (2002) Genetic control by a metabolite binding mRNA. Chem Biol 9:1043–1049

Navarro-Avilés G, Jiménez MA, Pérez-Marín MC, González C, Rico M, Murillo FJ, Elías-Arnanz M, Padmanabhan S (2007) Structural basis for operator and antirepressor recognition by *Myxococcus xanthus* CarA repressor. Mol Microbiol 63:980–994

Ortega A, Garcia de la Torre J (2003) Hydrodynamic properties of rodlike and disklike particles in dilute solution. J Chem Phys 114:9914–9919

Ortega A, Amoros D, Garcia de la Torre J (2011) Prediction of hydrodynamic and other solution properties of rigid proteins from atomic- and residue-level models. Biophys J 101:892–898

Ortiz-Guerrero JM, Polanco MC, Murillo FJ, Padmanabhan S, Elias-Arnanz M (2011) Light-dependent gene regulation by a coenzyme B_{12}-based photoreceptor. Proc Natl Acad Sci U S A 108:7565–7570

Pérez-Marín MC, Padmanabhan S, Polanco MC, Murillo FJ, Elías-Arnanz M (2008) Vitamin B_{12} partners the CarH repressor to downregulate a photoinducible promoter in *Myxococcus xanthus*. Mol Microbiol 67:804–819

Peselis A, Serganov A (2012) Structural insights into ligand binding and gene expression control by an adenosylcobalamin riboswitch. Nat Struct Mol Biol 19:1182–1184

Roth JR, Lawrence JG, Bobik TA (1996) Cobalamin (coenzyme B_{12}): synthesis and biological significance. Annu Rev Microbiol 50:137–181

Schuck P (2000) Size-distribution analysis of macromolecules by sedimentation velocity ultracentrifugation and Lamm equation modeling. Biophys J 78:1606–1619

Schuck P (2010a) Sedimentation patterns of rapidly reversible protein interactions. Biophys J 98:2005–2013

Schuck P (2010b) Diffusion of the reaction boundary of rapidly interacting macromolecules in sedimentation velocity. Biophys J 98:2741–2751

Schwartz PA, Frey PA (2007) 5′-Peroxyadenosine and 5′-peroxyadenosylcobalamin as intermediates in the aerobic photolysis of adenosylcobalamin. Biochemistry 46:7284–7292

Taga ME, Larsen NA, Howard-Jones AR, Walsh CT, Walker GC (2007) BluB cannibalizes flavin to form the lower ligand of vitamin B_{12}. Nature 446:449–453

Takano H, Kondo M, Usui N, Usui T, Ohzeki H, Yamazaki R, Washioka M, Nakamura A, Hoshino T, Hakamata W et al (2011) Involvement of CarA/LitR and CRP/FNR family transcriptional regulators in light-induced carotenoid production in *Thermus thermophilus*. J Bacteriol 193:2451–2459

Vistica J, Dam J, Balbo A, Yikilmaz E, Mariuzza RA, Rouault TA, Schuck P (2004) Sedimentation equilibrium analysis of protein interactions with global implicit mass conservation constraints and systematic noise decomposition. Anal Biochem 326: 234–256

Warren MJ, Raux E, Schubert HL, Escalante-Semerena JC (2002) The biosynthesis of adenosylcobalamin (vitamin B_{12}). Nat Prod Rep 19:390–412

Zhao H, Balbo A, Brown PH, Schuck P (2011) The boundary structure in the analysis of reversibly interacting systems by sedimentation velocity. Methods 54:16–30

Zoltowski BD, Crane BR (2008) Light activation of the LOV protein vivid generates a rapidly exchanging dimer. Biochemistry 47:7012–7019